Chapter 6

Squeeze Film in Curved Porous Circular Plates with Various Porous Structures

Contents

6.1 Introduction

Wu [108], in an innovative analysis, dealt with the case of squeeze film behavior for porous annular disks in which he showed that owing to the fact that fluid can flow through the porous material as well as through the space between the bounding surfaces, the performance of a porous walled squeeze film can differ substantially from that of a solid walled squeeze film. Murti [54] analyzed the squeeze film behavior between porous circular discs.

With the advent of ferrofluid (FF), Agrawal [1] studied its effects on a porous inclined bearing and found that the magnetization of the magnetic particles in the lubricant increased its load capacity without affecting the friction on the moving slider. Later Verma [103] and Shah and Bhat [78, 93] investigated the squeeze film between porous plates and found that its performance with magnetic fluid (MF) lubricant was better than with conventional lubricant.

In all above investigations, none of the authors considered various porous structures for porous plates (or discs or surfaces) in their study. The porous layer (or matrix or region) in the bearing is considered because its advantages property of self lubrication. With this motivation, we recapitulate the study of the paper of Shah and Bhat [87] for various porous structures without the effect of rotation, and with the effect of FF as lubricant under a magnetic field oblique to the lower plate. The problem also include the effect of squeeze velocity and the curvature of the upper disc. The FF flow model considered here is due to R. E. Rosensweig [74].

A FF lubrication equation is derived for the above problem and the various porous structures are considered for computation of bearing characteristics like pressure and load capacity. The FF used in computations are water based.

6.2 Formulation of Mathematical Model

The configuration of the bearing, shown in Figure 6.1, consists of two circular plates each of radius a. The upper plate has a porous facing of thickness l_1 which is backed by a solid wall. It moves normally towards an impermeable and flat lower plate with uniform velocity $\dot{h}_0 = dh_0/dt$, where h_0 is the central film thickness and t is time. The film thickness h is given by

$$h = h_0 \exp(-\beta r^2),$$

… (6.1)

where β is the curvature of the upper plate and r is the radial coordinate.

Assuming axially symmetric flow of the FF between the plates under an oblique magnetic field $\mathbf{H} = (H(r)\cos\phi, 0, H(r)\sin\phi)$, whose magnitude H vanishes at $r = 0, a$ and its strength H is defined as

$$H^2 = \frac{Kr^2(a-r)}{a},$$

… (6.2)

where $K = 10^{14}$ to 10^{16} is chosen so as to have a magnetic field of strength between the order of 10^5 to 10^6.

The angle $\phi = \phi(r, z)$, since the magnetic field arise out of a potential, can be determined from

$$\cot\phi\frac{\partial\phi}{\partial r} + \frac{\partial\phi}{\partial z} = \frac{3r-2a}{2r(a-r)},$$

… (6.3)

with the help of elliptic integrals depending on the value of a.

The modified Reynolds's type equation governing the film pressure p using basic equations (2.11) to (2.15) is [87]

$$\frac{1}{r}\frac{d}{dr}\left\{(h^3 + 12\psi l_1)r\frac{d}{dr}(p - 0.5\mu_0\bar{\mu}H^2)\right\} = 12\eta\dot{h}_0\,,$$

… (6.4)

where ψ is the permeability of the porous region, μ_0 is free space permeability, $\bar{\mu}$ is magnetic susceptibility, η is fluid viscosity and p is the pressure of fluid in the film region.

6.3 Solution of Case Studies

Case I (a globular sphere model as shown in Figure 6.2).

A porous material is filled with globular particles (a mean particle size D_c). In this case Kozeny-Carman formula [42] gives the permeability

$$\psi = \frac{D_c^2 \varepsilon^3}{180(1-\varepsilon)^2},$$

… (6.5)

where ε is the porosity.

Introduce the dimensionless quantities

$$\bar{p} = -\frac{p h_0^3}{\eta a^2 \dot{h}_0}, \quad R = \frac{r}{a}, \quad \overline{\psi} = \frac{D_c^2 l_1}{h_0^3}, \quad \bar{\beta} = \beta a^2, \quad \mu^* = -\frac{\mu_0 \bar{\mu} h_0^3 K}{\eta \dot{h}_0},$$

… (6.6)

Using equations (6.1), (6.2), (6.4), (6.5) and (6.6), the dimensionless film pressure $\bar{p}$ satisfies the equation

$$\frac{1}{R}\frac{d}{dR}\left\{\left(R\exp(-3\bar{\beta}R^2) + \frac{R\overline{\psi}\varepsilon^3}{15(1-\varepsilon)^2}\right)\frac{d}{dR}\left(\bar{p} - 0.5\mu^* R^2(1-R)\right)\right\} = -12.$$

… (6.7)

Solving equation (6.7) under the boundary conditions

$$\bar{p} = 0 \text{ when } R = 1 \text{ and } \frac{d\bar{p}}{dR} = 0 \text{ when } R = 0,$$

… (6.8)

one obtain

$$\bar{p} = 0.5\mu^* R^2(1-R) + \frac{15(1-\varepsilon)^2}{\overline{\psi}\bar{\beta}\varepsilon^3} ln\left\{\frac{15(1-\varepsilon)^2 + \overline{\psi}\varepsilon^3 \exp(3\bar{\beta})}{15(1-\varepsilon)^2 + \overline{\psi}\varepsilon^3 \exp(3\bar{\beta}R^2)}\right\}.$$

… (6.9)

The load capacity W of the bearing can be expressed in dimensionless form as

$$\bar{W} = -\frac{Wh_0^3}{2\pi\eta a^4 \dot{h}_0} = \frac{\mu^*}{40} + \int_0^1 \frac{15R(1-\varepsilon)^2}{\overline{\psi}\bar{\beta}\varepsilon^3} ln\left\{\frac{15(1-\varepsilon)^2 + \overline{\psi}\varepsilon^3 \exp(3\bar{\beta})}{15(1-\varepsilon)^2 + \overline{\psi}\varepsilon^3 \exp(3\bar{\beta}R^2)}\right\} dR.$$

… (6.10)

Case II (a capillary fissures model as shown Figure 6.3).

The model is composed of three sets of mutually orthogonal fissures (a mean solid size D_s), and assuming no loss of hydraulic gradient at the junctions, Irmay [31] derived the permeability

$$\psi = \frac{(1-m^{\frac{2}{3}})D_s^2}{12m},$$

… (6.11)

where $m = 1 - \varepsilon$.

Introduce the dimensionless quantities

$$\bar{p} = -\frac{ph_0^3}{\eta a^2 \dot{h}_0}, \quad R = \frac{r}{a}, \quad \overline{\psi} = \frac{D_s^2 l_1}{h_0^3}, \quad \bar{\beta} = \beta a^2, \quad \mu^* = -\frac{\mu_0 \bar{\mu} h_0^3 K}{\eta \dot{h}_0},$$

… (6.12)

Using equations (6.1), (6.2), (6.4), (6.11) and (6.12), the dimensionless film pressure $\bar{p}$ satisfies the equation

$$\frac{1}{R}\frac{d}{dR}\left\{\left(R\exp(-3\bar{\beta}R^2) + \frac{R\overline{\psi}(1-m^{\frac{2}{3}})}{m}\right)\frac{d}{dR}\left(\bar{p} - 0.5\mu^* R^2(1-R)\right)\right\} = -12.$$

… (6.13)

Solving equation (6.13) under the boundary condition (6.8), we obtain

$$\bar{p} = 0.5\mu^* R^2(1-R) + \frac{m}{\overline{\psi}\bar{\beta}(1-m^{\frac{2}{3}})} ln\left\{\frac{m + (1-m^{\frac{2}{3}})\overline{\psi}\exp(3\bar{\beta})}{m + (1-m^{\frac{2}{3}})\overline{\psi}\exp(3\bar{\beta}R^2)}\right\}.$$

… (6.14)

The load capacity W of the bearing can be expressed in dimensionless form as

$$\overline{W} = -\frac{Wh_0^3}{2\pi\eta a^4 \dot{h}_0} = \frac{\mu^*}{40} + \int_0^1 \frac{mR}{\overline{\psi}\bar{\beta}(1-m^{\frac{2}{3}})} ln\left\{\frac{m + (1-m^{\frac{2}{3}})\overline{\psi}\exp(3\bar{\beta})}{m + (1-m^{\frac{2}{3}})\overline{\psi}\exp(3\bar{\beta}R^2)}\right\} dR.$$

… (6.15)

6.4 Results and Discussion

The dimensionless pressure $\bar{p}$ and load capacity $\overline{W}$ are given, by equations (6.9), (6.10) for globular sphere model given by Kozeny-Carman and by equations (6.14), (6.15) for capillary fissures model by Irmay.

Setting the magnetization parameter $\mu^* = 0$ and without considering the two cases of ψ, the present analysis reduces to non-magnetic case [8].

Also, setting $\bar{\beta} = 0$ in equations (6.9), (6.10) and (6.14), (6.15), we obtain the results for flat upper plate for two cases.

The computed values of the dimensionless load capacity $\overline{W}$ are displayed in Figure 6.4 and Figure 6.5 for two different cases and for the following value of the parameters:

$$\varepsilon = 0.2,\ \ l_1 = 0.5(m),\ \ h_0 = 2.5 \times 10^{-5}(m),\ \ D_c = D_s = 0.000001(m),$$
$$\mu_0 = 4\pi \times 10^{-7}(N/A^2),\ \ \bar{\mu} = 0.05,\ \ \dot{h} = -0.005(m/s),$$
$$\eta = 0.012(Ns/m^2),\ \ a = 0.05(m),$$

Figure 6.4 and Figure 6.5 show that $\overline{W}$ increase with $\mu^*$and $\bar{\beta}$. The increases are substantial in the case of concave plates ($\bar{\beta} > 0$) for case I.

The load capacity also increases more in case I, this may be because of the slow coming out of the FF from the porous region.

6.5 Conclusion

Based upon the results and discussion it can be concluded that the better load carrying capacity is obtained for globular sphere model with the effect of FF under an oblique magnetic field to the lower plate.

Thus, it is suggested to have a design of porous squeeze bearing with globular sphere in the porous region.

6.6 Figures

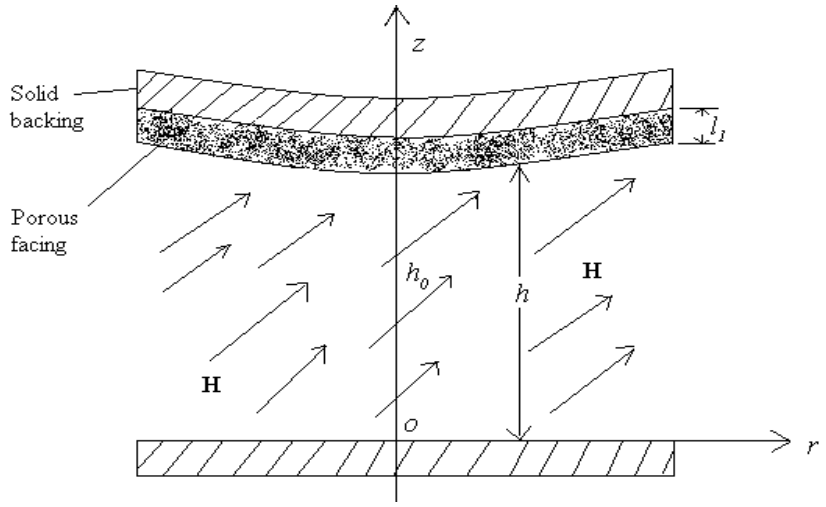

Figure 6.1 Configuration of the problem

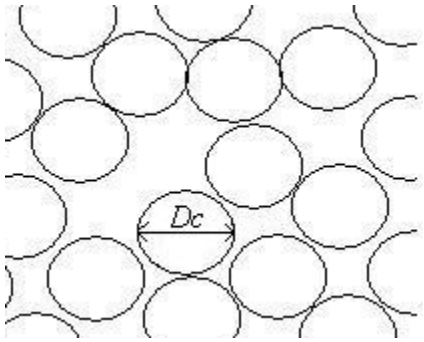

Figure 6.2 Structure model of porous sheets given by Kozeny-Carman

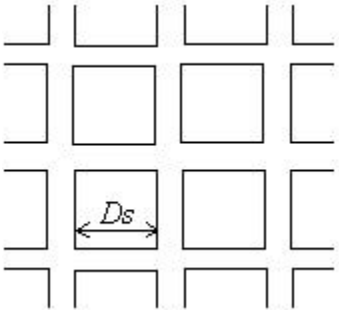

Figure 6.3 Structure model of porous sheets given by Irmay

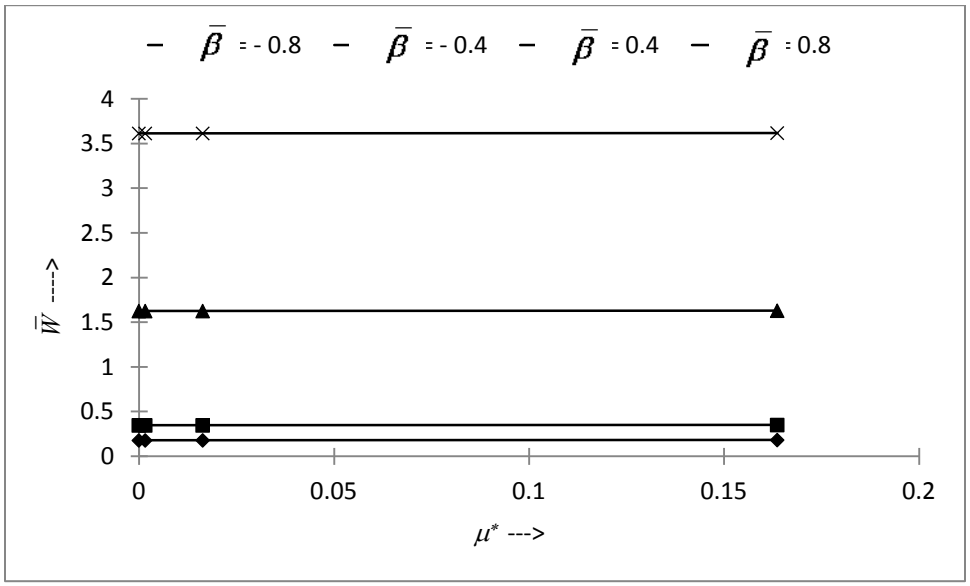

Figure 6.4 Values of the dimensionless load capacity $\bar{W}$ for different values of μ^* and $\bar{\beta}$ for case I

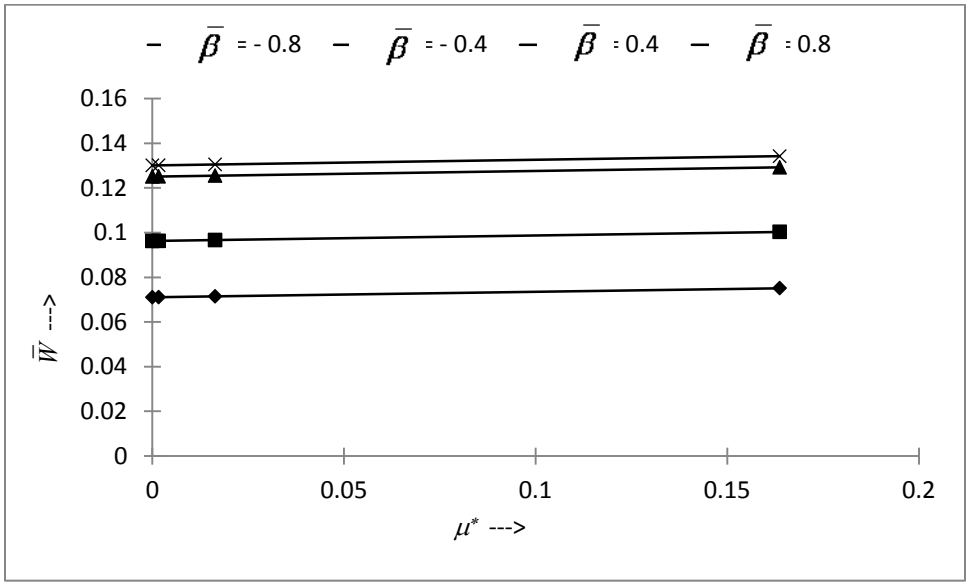

Figure 6.5 Values of the dimensionless load capacity $\bar{W}$ for different values of μ^* and $\bar{\beta}$ for case II